

Transport control in fusion plasmas by changing electric and magnetic field spatial profiles

T. Kroetz^a, F.A. Marcus^b, M. Roberto^a, I.L. Caldas^b, R.L. Viana^{c,*}, E.C. da Silva^b

^a Instituto Tecnológico de Aeronáutica, Centro Técnico Aeroespacial, Departamento de Física, 12228-900, São José dos Campos, São Paulo, Brazil

^b Instituto de Física, Universidade de São Paulo, 05315-970, São Paulo, São Paulo, Brazil

^c Departamento de Física, Universidade Federal do Paraná, 81531-990, Curitiba, Paraná, Brazil

ARTICLE INFO

Article history:

Received 4 September 2008

Received in revised form 25 November 2008

Accepted 18 December 2008

Available online 25 December 2008

PACS:

52.55.Fa

52.55.Dy

52.25.Gj

Keywords:

Plasma physics

Magnetic field lines

Tokamaks

ABSTRACT

For magnetically confined plasmas in tokamaks, we have numerically investigated how Lagrangian chaos at the plasma edge affects the plasma confinement. Initially, we have considered the chaotic motion of particles in an equilibrium electric field with a monotonic radial profile perturbed by drift waves. We have showed that an effective transport barrier may be created at the plasma edge by modifying the electric field radial profile. In the second place, we have obtained escape patterns and magnetic footprints of chaotic magnetic field lines in the region near a tokamak wall with resonant modes due to the action of an ergodic magnetic limiter. For monotonic plasma current density profiles we have obtained distributions of field line connections to the wall and line escape channels with the same spatial pattern as the magnetic footprints on the tokamak walls.

© 2008 Elsevier B.V. All rights reserved.

1. Introduction

In the program to develop the controlled thermonuclear fusion, tokamaks have been used to carry out experiments with magnetically confined plasmas [1]. In the last years it became evident that the plasma confinement strongly depends on the confining electric and magnetic fields spatial profiles at the plasma edge [2]. The influence of these fields on the plasma wall interaction, the plasma edge electrostatic turbulence, and the anomalous particle transport induced by this turbulence are nowadays under investigation in all tokamaks. As for the magnetic fields, chaotic field lines at the plasma edge have been found to play a key role on plasma-wall interaction in tokamaks [3–5]. Since charged plasma particles follow magnetic field lines to leading order, one of the undesirable effect of chaotic field lines is the concentration of heat and particle loadings on the tokamak wall that deteriorates the overall plasma confinement quality [6–8]. These topics are among the main investigations to be addressed in the new tokamak ITER that has been designed to achieve plasma conditions required in a nuclear fusion reactor. Thus, it is important to consider the influence on particle transport due to these complementary kinds of particle motion.

Furthermore, the anomalous particle transport induced by the plasma edge turbulence arises from some combination of the electric and magnetic fields [9]. Hence a comprehensive description of the observed anomalous particle transport has to take into account the electric and magnetic field spatial profiles at plasma edge. The complexity of the energy transfer between waves and particles makes difficult a direct attack to this problem by, e.g., computer codes based on a kinetic description of particles interacting with electric and magnetic fields chaotic in space and time. In spite of such difficulties, some common issues exist such that we can grasp some physically interesting issues from the isolated analysis of chaotic magnetic and electric fields. These conservative fields can be described by Hamiltonian systems with chaotic solutions [10].

Our main goal in this paper is to investigate effects from electric and magnetic sheared fields on plasma confinement through a combination of numerical simulation results and concepts from Hamiltonian dynamics theory. In the plasma edge, shear occurs for the equilibrium electric field radial profile related to drift wave dispersion relation. In fact, this field causes a $\mathbf{E} \times \mathbf{B}$ force which drives particle drift flow modifying the experimentally observed particle transport [2,9]. We performed numerical simulations of particle motion by solving the canonical equations from a drift-kinetic Hamiltonian considering the action of two waves with a phase-difference, which leads to a non-integrable system, for which there are periodic, quasi-periodic, and chaotic trajectories. We showed

* Corresponding author.

E-mail address: viana@fisica.ufpr.br (R.L. Viana).

that, by modifying the electric field profile, particle transport can be reduced by the displacement of barriers at the plasma edge.

Concerning the magnetic sheared equilibrium field we have added the field of an ergodic magnetic limiter so as to generate non-integrable field line configurations and Lagrangian chaos. Our numerical simulations used parameters taken from the Brazilian tokamak TCABR, for which an ergodic limiter has been designed to control plasma oscillations [11,25]. Thus, we showed that the magnetic line escape to the wall depends on the equilibrium and resonance parameters and presents a magnetic footprint similar to those recently observed for discharges in tokamaks with chaotic field lines [13,14]. As far as other tokamaks are concerned, ergodic limiters have been used to improve plasma confinement in TEXT-UPGRADE [5], TORE SUPRA [12], TEXTOR [13], and DIII-D [14].

Our analysis is based on numerical algorithms used in chaos theory to investigate and describe chaotic orbits and the creation and destruction of transport barriers. One of these algorithms consists on the obtention of area-preserving Poincaré maps for both magnetic field lines and particle drift trajectories [10]. Another kind of algorithms we have used to analyze our results is for the numerical obtention of homoclinic tangles. Since the latter represent highly unstable invariant sets, the numerical procedure to obtain them must carefully avoid the divergence of orbits near the hyperbolic points due to the chaotic nature of the orbit [15,16]. Moreover, the chaotic orbits were integrated for a very long time in order to obtain the recurrence and escape properties described in the paper. Without the adoption of these algorithms to our problems in tokamak plasma, the presented results could not have been obtained.

The rest of this paper is organized as follows: in Section 2 we consider the electric sheared configuration through the interaction of particles with one and two electrostatic waves in a uniform magnetic field. Section 3 deals with the magnetic sheared case by presenting the model fields for the tokamak equilibrium field and the ergodic limiter perturbation, for the obtention of a field line map, and our numerical results concerning escape patterns and magnetic footprints. Our conclusions are left to the last section.

2. Particle transport barriers

Experiments indicate that the plasma edge behavior depends on the anomalous particle transport caused by the observed electrostatic turbulence [9]. Thus, it is important to estimate the contribution to this transport due to chaotic particle orbits driven by the turbulent fluctuation. To do that, in this work we study the transport of particles in a magnetically confined plasma, due to electrostatic drift waves. The adopted model describes the trajectory of the guiding center of a particle in a uniform magnetic field perpendicular to a radial electric field perturbed by drift waves, using the Hamiltonian description for the guiding center trajectory [17].

The $\mathbf{E} \times \mathbf{B}$ drift produced by the equilibrium radial electric field and a dominant wave is represented by the integrable part of the Hamiltonian, while the other part contains the perturbation representing the fluctuating electric field associated to other drift waves. We study the resonances and island chains, created at the plasma edge and associate the anomalous plasma edge transport to the Lagrangian chaotic transport of the guiding centers of ions [17]. In this way we obtain chaotic orbits that determine the particle radial transport, based on experimental data obtained in tokamaks to get numerically realistic predictions [18,19].

Single particle motion in one drift wave is described by an integrable Hamiltonian system and can be solved analytically. For a resonant wave, the phase space around a two-dimensional lattice of counter rotating rolls separated by a separatrix is created in the resonant region. The particles cannot cross the separatrix so

that they are confined to motion within a single roll [17]. The second wave, with an amplitude smaller than that of the first wave, is treated as a perturbation. The Hamiltonian is no longer time-independent such that a particle is no longer confined to a single roll [17]. Thus, qualitative features of this transport can be approximated by a low-dimensional dynamical system with island chains in phase space due to the superposition of two dominant drift waves.

We describe the superposition of poloidal drift waves as a Hamiltonian system. The drift velocity of the guiding centers are given by [17]:

$$\mathbf{v} = -\frac{\nabla\phi \times \mathbf{B}}{B^2}, \quad (1)$$

which is equivalent to the following set of differential equations:

$$v_x = \frac{dx}{dt} = -\frac{1}{B_0} \frac{\partial\phi(x, y, t)}{\partial y}, \quad (2)$$

$$v_y = \frac{dy}{dt} = \frac{1}{B_0} \frac{\partial\phi(x, y, t)}{\partial x}, \quad (3)$$

representing canonical equations obtained from the Hamiltonian as

$$H(x, y, t) = \frac{1}{B_0} \phi(x, y, t). \quad (4)$$

Here we consider the drift wave caused by two waves. Using dimensionless variables in a frame moving with the plasma phase velocity of the first wave, we obtain the Hamiltonian

$$H(x, y, t) = \phi_0(x) - u_1 x + A_1 \sin(k_{x1}x) \cos(k_{y1}y) + A_2 \sin(k_{x2}x) \cos(k_{y2}(y - ut)), \quad (5)$$

where $u = \omega_2/k_{y2} - \omega_1/k_{y1}$ is the phase velocity difference between the second and the first waves, and $u_1 = \omega_1/k_{y1}$. x and y correspond to radial and poloidal coordinates.

When the system has only one wave ($A_2 = 0$), the Hamiltonian is integrable. In this case it is relevant the dimensionless trapping profile U [17]:

$$U(x) = \frac{1}{A_1 k_{x1}} \left[\frac{d\phi_0(x)}{dx} - u_1 \right] \sim v_E - u_1, \quad (6)$$

which gives how sensitive is the background equilibrium system to the second wave perturbation and how intense the radial transport would be [19].

In order to investigate the effects of electric field we choose a potential with a monotonic radial profile

$$\phi_0(x) = Ax^2 + Bx, \quad (7)$$

where the parameters A and B can be adjusted by the electric potential profile of a tokamak discharge. Consequently, from the choice of the electric potential in Eq. (7), the trapping parameter becomes

$$U(x) = \frac{1}{A_1 k_{x1}} (2Ax + B - u_1). \quad (8)$$

Fig. 1 depicts two $U(x)$ linear profiles as a function of the radial position x normalized by the plasma radius. In this figure the profile described by the dashed line has the extreme values of U near to 0.8, and for the dot dashed line the extreme values are around 1.3. Superposition of two waves lend us to chaotic scenery. It is important to notice the grid of islands and the influence of the second wave for arising the chaos [19]. We analyze the influence of presence of the second wave for the two different electric field profiles.

From the previous work done with constant electric potential profile [9,17,18,20], it is known that the islands chain cover entirely the phase space when $U(x) = 0$ and this is the configuration with

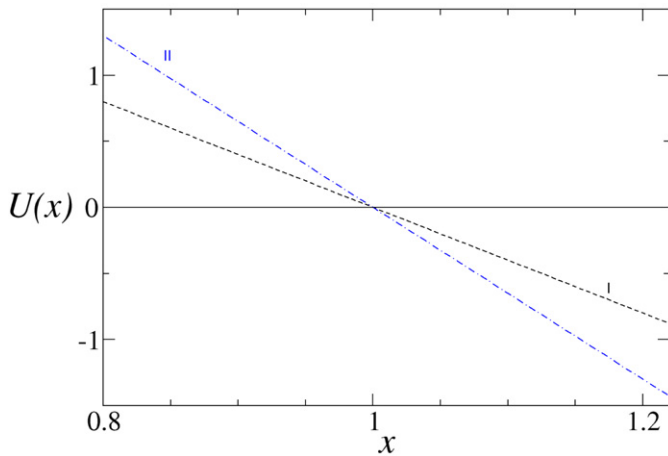


Fig. 1. Radial profiles I (dashed line) and II (dot-dashed line) of the trapping parameter $U(r)$ for the case of a monotonic electric field.

the highest transport rate. It is also reported that for $U(x) = 0$ we have a resonant condition, $v_E = u_1$. This means that the poloidal drift velocity is equal to the wave phase velocity, $(1/B_0)\phi'_0 = u_1$, which is also confirmed by experiments in tokamaks [21]. Fig. 2(a) shows the configuration of the islands with one wave. It is important to notice the presence of the barriers at $x = 0.8$ and $x = 1.2$ where the trapping profile is maximum for $U_{\max} = 0.8$. These barriers describe a zonal flow. Fig. 2(b) shows how the transport depends on the grid of the first wave islands and the second wave amplitude. Moreover, we can see that the particles describe chaotic motion above and below the zonal flow and around the elliptic points.

As the electric potential in Eq. (7) increases by the change of the parameters A and B , we notice in Fig. 3(a) a stronger flow takes place at the extreme regions at $x = 0.85$ and $x = 1.2$, and also a island size reduction inside the flows. The resonant condition, $u_1 = E_x$ occurs at those radii \bar{x} given by $U(\bar{x}) = 0$.

Fig. 2(a) depicts a phase space plot for the integrable Hamiltonian system consisting of the profile I and one wave ($A_2/A_1 = 0$). Without the second wave there is no chaos and the phase space exhibits some periodic structures where $U \approx 0$, consisting on islands chains centered at fixed points. The particular island chain, occurring at the radial location wherein $U(\bar{x}) = 0$, turns to be the place where the second wave acts more intensively generating a chaotic layer. Such a resonant island chain occurs at $\bar{x} \approx 1.0$. Complementary, in the region where $|U| < 1$ the phase space is mixed with partial barriers separating small island.

The superposition of two drift waves turns the Hamiltonian system a non-integrable one, with the consequent breakdown of a number of invariant curves (in the phase plane) and the consequent formation of homoclinic chaos. Fig. 2(b) shows the perturbed phase plot obtained by adding a second wave with amplitude $A_2/A_1 = 0.2$ to the integrable system of one wave. The separatrix orbits connecting the hyperbolic-points are the first ones to become chaotic when the second wave is added. The orbits near the elliptic points remain closed, while orbits near the hyperbolic points are chaotic, filling some nonzero area in the phase plane with a bounded radial excursion, thus contributing to particle diffusion along this direction. Small islands of stability still exist near the elliptic points, but large scale transport takes place due to the more pronounced radial excursion of orbits throughout the chaotic layer. The partial barriers are broken and cannot limit the particle radial transport in this region.

In Figs. 3(a) and 3(b) we consider the equilibrium profile II for one and two waves, respectively. We see that an additional barrier appear in the region for which $U \approx 1$ separating the island

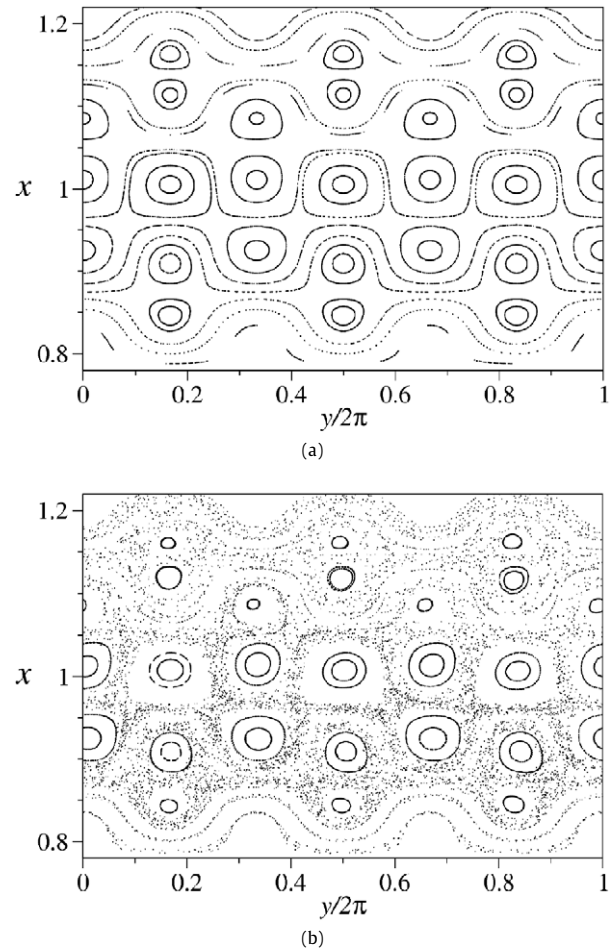


Fig. 2. Increase of ergodicity with the wave-amplitude ratio. (a) First wave islands and the zonal flow for $U_{\max} = 0.85$, $A_2/A_1 = 0$ in $x \times y$ plane. (b) Two waves, $A_2/A_1 = 0.2$, with zonal flow at $x = 0.85$ and $x = 1.2$.

chains seen in the previous figures. This barrier appears due to the electric field shear increase according to the profile II. As a consequence of this variation, the orbit ergodization is reduced to the internal part of the plasma edge. This result shows that the transport can be reduced by changing the radial electric field profile, such that $|U| > 1$.

3. Escape patterns of magnetic field lines

A second problem related to transport control in fusion plasmas is the study of the field line escape that reach the tokamak wall. The field lines are determined by the superposition of two magnetic fields; one in the toroidal direction and the other in the poloidal direction. The superposition of these fields produces magnetic field lines with a helical shape, lying on constant pressure surfaces called magnetic surfaces, with topology of nested tori [1]. As we have a toroidal symmetry, the equilibrium quantities do not depend on azimuthal angle φ . The magnetic field line equation can be viewed as Hamilton equations describing an integrable system, where the angle φ plays the role of time. Introducing a small helical magnetic perturbation, the Hamiltonian system becomes almost-integrable [2,22]. In this work we use an ergodic magnetic limiter (EML) to generate a small localized perturbation, where the explicit dependence on φ reflects the break of symmetry [5,23–26]. The EML creates resonances in the plasma and it can be designed to excite resonances closer or farther from the toka-

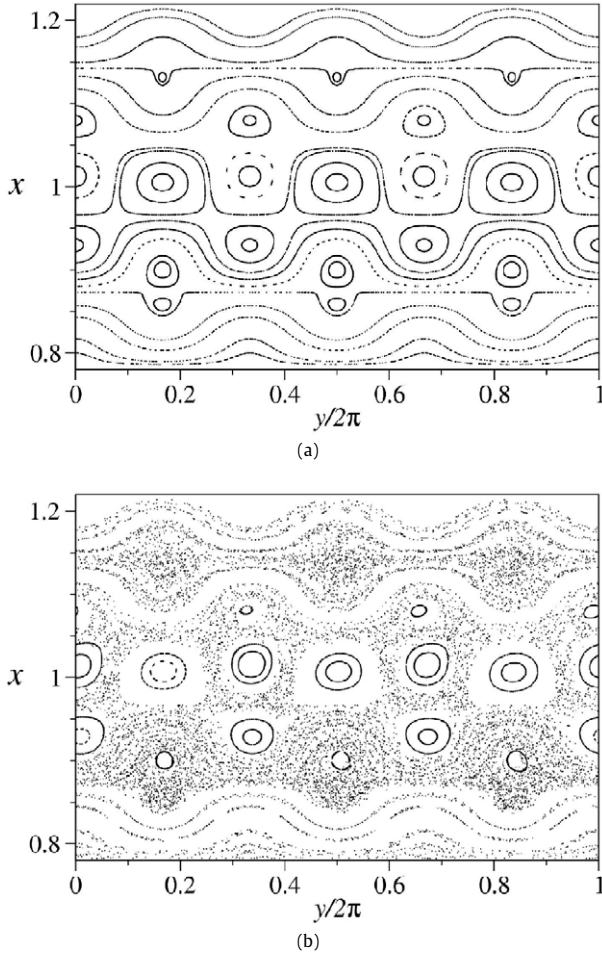


Fig. 3. Increase of ergodicity with the wave-amplitude ratio. (a) First wave islands and the zonal flow for $U_{\max} = 1.30$, $A_2/A_1 = 0$ in $x \times y$ plane. (b) Two waves, $A_2/A_1 = 0.2$, with zonal flow at $x = 0.85$ and $x = 1.2$.

mak wall, depending on the mode numbers chosen for the limiter winding.

First of all we describe the equilibrium magnetic field lines, choosing an appropriate coordinate system. The choice of this system is determined by the symmetries exhibited by the system. For the so-called local coordinates (r, θ, φ) that are a kind of cylindrical coordinates with toroidal curvature, the coordinate surfaces $r = \text{constant}$ hardly coincide with actual equilibrium magnetic surfaces [1]. A better choice would be the toroidal coordinates (ξ, ω, Φ) [28], but their coordinate surfaces are not suitable as well. We have used in this paper a polar toroidal non-orthogonal coordinate system $(r_t, \theta_t, \varphi_t)$, given by [29]

$$r_t = \frac{R'_0}{\cosh \xi - \cos \omega}, \quad \theta_t = \pi - \omega, \quad \varphi_t = \Phi, \quad (9)$$

in terms of the usual toroidal coordinates (ξ, ω, Φ) , where R'_0 is the magnetic axis radius. They are related to the local (or pseudo-toroidal) coordinates (r, θ, φ) by the following relations

$$r_t = r \left[1 - \frac{r}{R'_0} \cos \theta + \left(\frac{r}{2R'_0} \right)^2 \right]^{1/2}, \quad (10)$$

$$\sin \theta_t = \sin \theta \left[1 - \frac{r}{R'_0} \cos \theta + \left(\frac{r}{2R'_0} \right)^2 \right]^{-1/2}, \quad (11)$$

such that, in the large aspect ratio limit ($r_t \ll R'_0$), r_t and θ_t become r and θ , respectively [29].

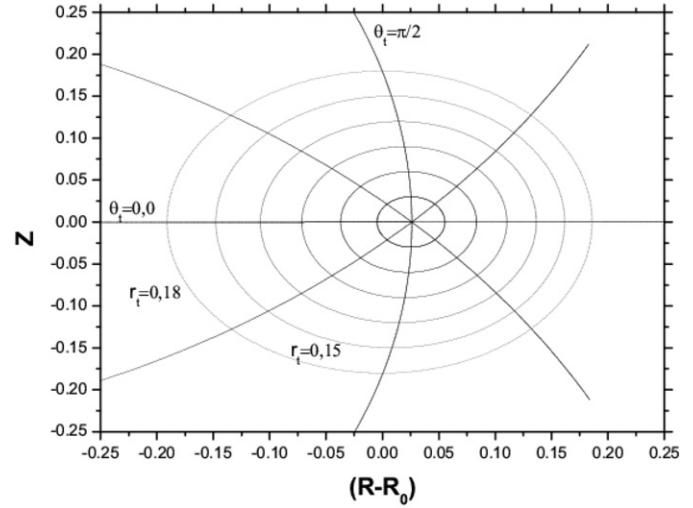


Fig. 4. Some coordinate surfaces of the polar toroidal coordinate system in the $\varphi = 0$ plane.

Fig. 4 shows some coordinate surfaces of the $(r_t, \theta_t, \varphi_t)$ system. Note that the $r_t = \text{const.}$ curves have a pronounced curvature in the interior region of the torus, from where we start counting poloidal θ_t angles. Moreover, the origins of these two coordinate systems are the magnetic axis. Finally, the relation of the magnetic axis radius R'_0 with the coordinate R is

$$R^2 = R'^2_0 \left[1 - 2 \frac{r_t}{R'_0} \cos \theta_t - \left(\frac{r_t}{R'_0} \right)^2 \sin^2 \theta_t \right]. \quad (12)$$

The equilibrium magnetic fields in tokamaks can be obtained from MHD equilibrium theory. The expansion caused by a pressure gradient is counter-balanced by the Lorentz force produced by the plasma current density. Thus, the equilibrium magnetic field lines lie on constant pressure surfaces, or magnetic surfaces. This property can be described by a scalar function, a surface quantity Ψ_p , such as $\mathbf{B}_0 \cdot \nabla \Psi_p = 0$, where \mathbf{B}_0 is the plasma equilibrium magnetic field and the magnetic surfaces are characterized by $\Psi_p = \text{constant}$ [1]. The tokamak equilibrium magnetic field \mathbf{B}_0 is obtained from an approximated analytical solution of the Grad–Schlüter–Shafranov equation in these coordinates [29], such as $\Psi_p \approx \Psi_p(r_t)$.

Thus, in the large aspect ratio limit the equilibrium flux function Ψ_p does not depend on θ_t . The intersections of the flux surfaces $\Psi_p = \text{constant}$ with a toroidal plane are not concentric circles but rather present a Shafranov shift toward the exterior equatorial region [29]. Hence, as commonly observed in tokamaks [1], equilibrium flux surfaces can be approximated by $r_t = \text{const.}$ coordinate surfaces. In this large aspect limit case, the Grad–Schlüter–Shafranov equation simplifies as

$$\frac{1}{r_t} \frac{d}{dr_t} \left(r_t \frac{d\Psi_p}{dr_t} \right) = \mu_0 J(\Psi_p), \quad (13)$$

where J is the toroidal component of the equilibrium plasma current density. In this work we have used a toroidal peaked current density profile, commonly observed in tokamaks discharges, given by [1]

$$J(r_t) = \frac{I_p R'_0}{\pi a^2} (\gamma + 1) \left(1 - \frac{r_t^2}{a^2} \right)^\gamma, \quad (14)$$

where I_p and a are the total plasma current and plasma radius, respectively, and γ is a positive constant.

In this equilibrium, the contravariant components of the equilibrium field are given by

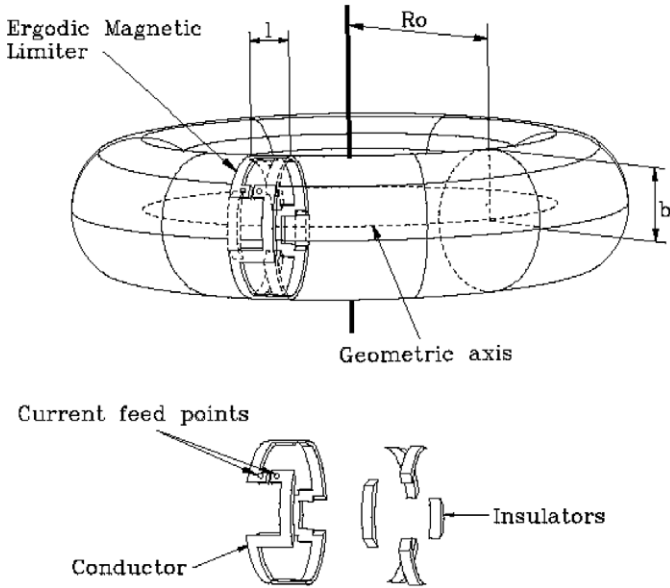


Fig. 5. Scheme of an ergodic magnetic limiter.

$$B_0^1(r_t, \theta_t) = -\frac{1}{R_0' r_t} \frac{\partial \Psi_p}{\partial \theta_t} = 0, \quad (15)$$

$$B_0^2(r_t, \theta_t) = \frac{1}{R_0' r_t} \frac{\partial \Psi_p}{\partial r_t} = \frac{\mu_0 I_p}{2\pi r_t^2} \left[1 - \left(1 - \frac{r_t^2}{a^2} \right)^{\gamma+1} \right], \quad (16)$$

$$B_0^3(r_t, \theta_t) = -\frac{\mu_0 I}{R^2} = \frac{\mu_0 I_e}{2\pi R_0'^2} \left[1 - 2 \frac{r_t^2}{R_0'} \cos \theta_t \right]^{-1}, \quad (17)$$

where $I_e \approx -I/2\pi$ is the total current in the toroidal field coils in the large aspect ratio approximation [26]. The field line revolutions along the torus can be calculated by using the rotational transform, given by $\iota = 2\pi d\theta_t/d\phi$. In fusion plasmas is conventionally used the safety factor $q(r_t)$ instead of rotational transform, such as, $\iota = 2\pi/q(r_t)$. The safety factor of the magnetic surfaces is given by,

$$q(r_t) = \frac{1}{2\pi} \int_0^{2\pi} \frac{B_0^3(r_t, \theta_t)}{B_0^2(r_t, \theta_t)} d\theta_t, \quad (18)$$

which results in a parabolic profile.

The design for the ergodic magnetic limiter to be considered in this paper is essentially the same as in Ref. [26], and consists of N_r current rings of length ℓ located symmetrically along the toroidal direction of the tokamak (Fig. 5). These current rings may be regarded as slices of a pair of external helical windings located at $r_t = b_t$, conducting a current I_h in opposite senses for adjacent conductors. The role of these windings is to induce a resonant perturbation in the tokamak, and to achieve this effect we must choose a helical winding with the same pitch as the field lines in the rational surface we want to perturb. This has been carried out by choosing the following winding law [26] $u_t = m_0(\theta_t + \lambda \sin(\theta_t)) - n_0\phi_t = \text{constant}$, where λ is a tunable parameter.

The magnetic field \mathbf{B}_L produced by the resonant helical winding, from which we build the EML rings, is obtained by neglecting the plasma response. In this case, \mathbf{B}_L is assumed to be a vacuum field, such that it comes from solving Laplace's equation with proper boundary conditions at the tokamak wall. We were able to obtain an approximated analytical solution, such that, in low-

est order, the only non-vanishing component of the corresponding vector potential is [26]

$$A_{L3}(r_t, \theta_t, \phi_t) = -\frac{\mu_0 I_h R_0'}{\pi} \left(\frac{r_t}{b_t} \right)^{m_0} \cos(m_0\theta_t - n_0\phi_t). \quad (19)$$

Since the equilibrium field is axisymmetric, it represents, in terms of the Hamiltonian description for the field line flow, an integrable dynamical system. We may set the azimuthal angle, $\phi_t = t$, as a time-like variable, and put field line equation in a Hamiltonian form

$$\frac{d\mathcal{J}}{dt} = -\frac{\partial H}{\partial \vartheta}, \quad (20)$$

$$\frac{d\vartheta}{dt} = \frac{\partial H}{\partial \mathcal{J}}, \quad (21)$$

where (\mathcal{J}, ϑ) are the action-angle variables of a Hamiltonian H . The action is defined in terms of the toroidal magnetic flux and the angle is a modified poloidal angle. These variables are given by [26]:

$$\mathcal{J}(r_t) = \frac{1}{2\pi R_0'^2 B_T} \int \mathbf{B}_0 \cdot d\sigma_3 = \frac{1}{4} \left[1 - \left(1 - 4 \frac{r_t^2}{R_0'^2} \right)^{1/2} \right], \quad (22)$$

$$\begin{aligned} \vartheta(r_t, \theta_t) &= \frac{1}{q(r_t)} \int_0^{\theta_t} \frac{B_0^3(r_t, \theta_t)}{B_0^2(r_t, \theta_t)} d\theta \\ &= \left[1 - 4 \frac{r_t^2}{R_0'^2} \right]^{1/2} \int_0^{\theta_t} \frac{d\theta}{1 - 2(r_t/R_0') \cos \theta} \\ &= 2 \arctan \left[\frac{1}{\Omega(r_t)} \left(\frac{\sin \theta_t}{1 + \cos \theta_t} \right) \right], \end{aligned} \quad (23)$$

where $d\sigma_3 = R_0' r_t dr_t d\theta_t \hat{\mathbf{e}}^3$ and

$$\Omega(r_t) = \left(1 - 2 \frac{r_t}{R_0'} \right)^{1/2} \left(1 + 2 \frac{r_t}{R_0'} \right)^{-1/2}. \quad (24)$$

The addition of the magnetic field produced by a resonant helical winding characterized by Eq. (19) may be regarded as a Hamiltonian perturbation

$$H(\mathcal{J}, \vartheta, t) = H_0(\mathcal{J}) + H_1(\mathcal{J}, \vartheta, t) \quad (|H_1/H_0| \ll 1) \quad (25)$$

$$= \frac{1}{B_T R_0'^2} \Psi_{p0}(\mathcal{J}) + \frac{1}{B_T R_0'^2} A_{L3}(\mathcal{J}, \vartheta, t). \quad (26)$$

In order to include the effect of the finite length ℓ of each EML ring, which is typically a small fraction of the total toroidal circumference $2\pi R_0'$, we model its effect as a sequence of delta-functions centered at each ring position [26]:

$$H_L(\mathcal{J}, \vartheta, t) = H_0(\mathcal{J}) + \frac{\ell}{R_0'} H_1(\mathcal{J}, \vartheta, t) \sum_{k=-\infty}^{+\infty} \delta\left(t - k \frac{2\pi}{N_a}\right), \quad (27)$$

where the N_a rings are symmetrically distributed in the toroidal direction.

We can derive, due to the impulsive perturbation, a stroboscopic map for field line dynamics, by defining \mathcal{J}_n and ϑ_n as the action and angle variables just after the n th kick due to a limiter ring at the toroidal positions $\phi_k = 2k\pi/N_r$, with $k = 0, 1, \dots, N_r - 1$ [26].

$$\mathcal{J}_{n+1} = \mathcal{J}_n + \epsilon f(\mathcal{J}_{n+1}, \vartheta_n, t_n), \quad (28)$$

$$\vartheta_{n+1} = \vartheta_n + \frac{2\pi}{N_r q(\mathcal{J}_{n+1})} + \epsilon g(\mathcal{J}_{n+1}, \vartheta_n, t_n), \quad (29)$$

$$t_{n+1} = t_n + \frac{2\pi}{N_r}, \quad (30)$$

where

$$f(\mathcal{J}, \vartheta, t) = -\frac{\partial H_1(\mathcal{J}, \vartheta, t)}{\partial \vartheta}, \quad (31)$$

$$g(\mathcal{J}, \vartheta, t) = \frac{\partial H_1(\mathcal{J}, \vartheta, t)}{\partial \mathcal{J}}, \quad (32)$$

and the perturbation intensity is

$$\epsilon = -2 \left(\frac{\ell}{2\pi R'_0} \right) \left(\frac{I_h}{I} \right), \quad (33)$$

which can be considered as a small parameter, since in experiments we usually have $\ell \ll 2\pi R'_0$ and $I_h \ll I$. This procedure has been successfully used to introduce relevant maps in different Hamiltonian systems. For example, the standard map describes a rotor perturbed by a periodic sequence delta function kicks similar to that used in our map [10]. Even so, those maps are obtained through the integration of differential equations involving delta functions, which can be ill-defined in some cases. However, there exists a rigorous method for deriving such mappings from equations with impulsive functions [27].

To apply these procedures to obtain the numerical simulations described in this paper, we choose an equilibrium characterized by the following parameters: $a/R'_0 = 0.28$ and $b/R'_0 = 0.35$, where a is the minor plasma radius, R'_0 is the major tokamak radius, corresponding to the magnetic axis, and b_t is the minor tokamak radius. We also choose $q(a) = 5.00$ and $q(0) = 1.05$, corresponding to the safety factors at the plasma edge and magnetic axis, respectively, for which $\gamma = 3.0$. For this equilibrium the monotonic safety factor profile in terms of the action variable is presented in Fig. 6.

We make the limiter field, with $N_a = 4$ rings, resonate with the magnetic surface with safety factor $q = 4.0$ or $q = 5.0$ by choosing the perturbation parameters as $\lambda = 0.5276$ and $\lambda = 0.5894$ and the mode numbers $(m_0/n_0 = 8/2)$ or $(10/2)$, respectively. Fig. 7 shows the Poincaré map for the $(8, 2)$ (a) and $(10, 2)$ (b) perturbations. For these cases the limiter currents are $I_h/I_p = 0.040$ and $I_h/I_p = 0.017$, respectively. In these figures the main resonance positions in the phase space are indicated by arrows with their rational values of the safety factor. The island chains due to these resonances although partially destroyed, can be recognized. In external part of the plasma there are mixed regions with islands and chaotic lines, while more inside the plasma whole magnetic surfaces can be identified.

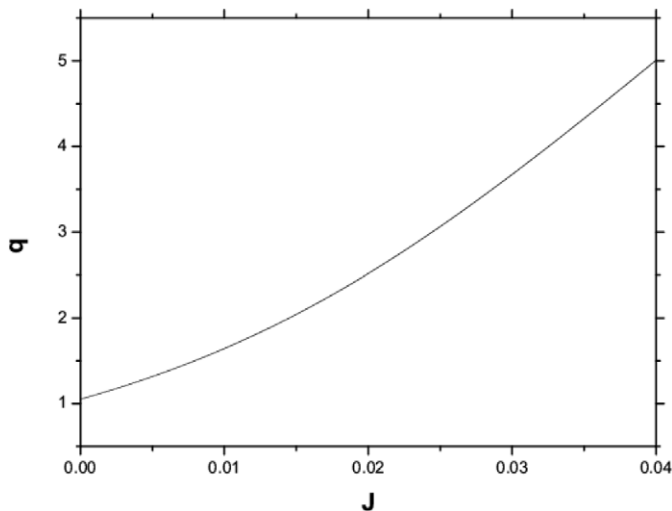


Fig. 6. Safety factor profile for equilibria with $\gamma = 3.0$. The minor radius of tokamak vessel is denoted by b .

The non-uniformity of the outer chaotic region due to an ergodic limiter can be described by the distribution of the connection lengths of field lines in the plasma edge. The connection length, $N_{cl}(r, \theta)$, is the number of toroidal turns it takes for a field line, originating from a given initial condition located at (r, θ) in the Poincaré section, to reach the tokamak wall. In our case we can set the tokamak wall at the same radius of the ergodic limiter rings, at $r_t = b_t$. The field line is considered lost when it reaches this radial position. The connection length indicates a rough estimate of the escape time for a particle, passing through the point (r, θ) , to hit the tokamak wall. Recent experiments have shown that the radial structure of the electron temperature and density at different times of the discharge reveals a correlation between the connection length and the heat flux [30]. There has been observed that most of the heat content is brought from the plasma core wall by the field lines with relatively large connection lengths (namely, those with $N_{cl} > 4$).

The connection length depends on the position at the chaotic region in the Poincaré section and, since the chaotic region is non-uniform, as shown in Figs. 7(a) and 7(b), we expect a non-uniform distribution of connection lengths in our system. We have numerically computed the distribution of the connection lengths for the maps of Figs. 7(a) and 7(b), by using grids of points on the chaotic region of the corresponding phase portraits, each point serving as

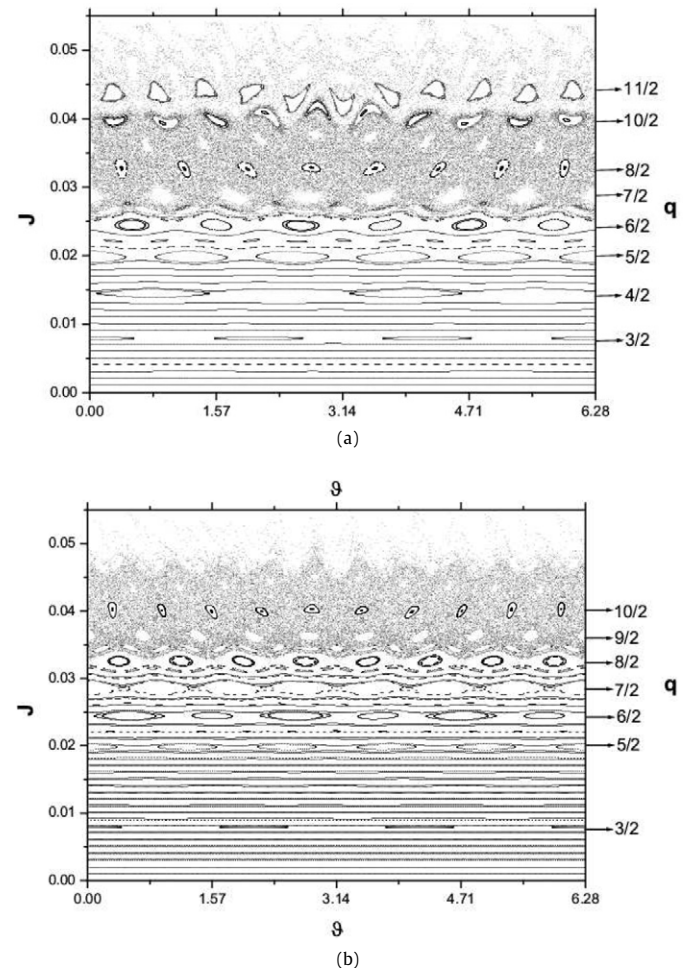


Fig. 7. Increase of ergodicity with the ratio between the perturbing current and the equilibrium plasma current. Poincaré section of a tokamak perturbed by an EML, for a safety factor profile with $\gamma = 3.0$, $N_r = 4$, (a) $(m_0, n_0) = (8, 2)$, $\lambda = 0.5276$, and $I_h/I_p = 0.040$, (b) $(m_0, n_0) = (10, 2)$, $\lambda = 0.5894$ and $I_h/I_p = 0.017$.

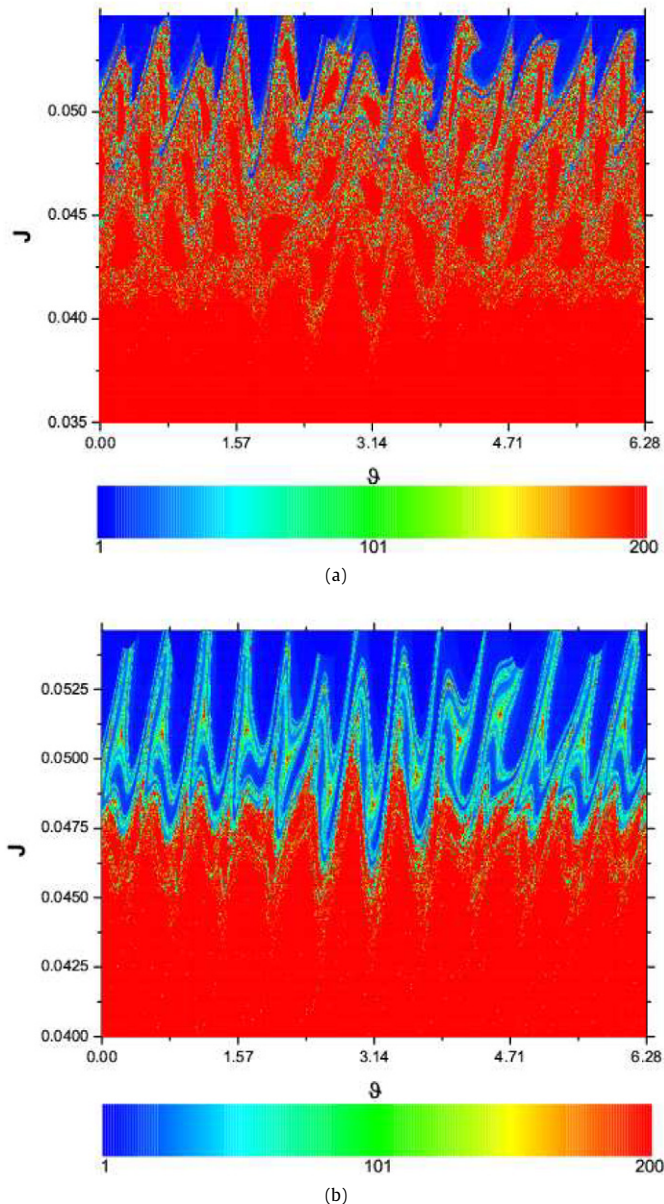


Fig. 8. Connection lengths in the range [1,200] for the Poincaré sections shown in Figs. 7(a) and 7(b). (For interpretation of the references to color in this figure legend, the reader is referred to the web version of this article.)

a different initial condition. In fact, the connection lengths take on values in a wide interval, from $N_{cl} = 1$ to $N_{cl} \approx 10^4$.

We depict, in Figs. 8(a) and 8(b), the connection lengths for each point of this grid, within intervals from 1 to 200 turns. For each interval, the number of turns are indicated by using a color scale. We have chosen a bounded radial portion of the toroidal section, since we are interested on the escape of the field lines near to the tokamak wall (initial conditions with $N_{cl} > 200$ belong altogether in black (brown on on-line version) regions). The regions with short and long connection lengths are also called *laminar* and *ergodic*, respectively. The laminar region is convenient for the purpose of the ergodic limiter, i.e., to isolate the plasma bulk from the wall. Thus, comparing the two ergodic limiters considered in this work we claim that the (10, 2) configuration is more appropriated since its laminar region is larger even for a lower current I_h considering in this work.

Moreover, fractal structures can be seen in Figs. 8(a) and 8(b). From these examples we can see that not only the connection lengths of the field lines are important, but also their radial penetration depths. For example, there are field lines with small connection lengths starting near the wall or in the vicinity of the island chains. Those field lines produce a quite uniform escape pattern, i.e. without a noticeable concentration on a given region of the wall, and hence should not contribute to the heating deposition patterns observed on the wall. The field lines around the islands with high penetration depth are more evident for the (8, 2) mode [Fig. 8(a)] than for the (10, 2) one [Fig. 8(b)]. Field lines with connection lengths higher than a given limit (say, $N_{cl} = 4000$), can be considered as effectively trapped. Hence a region with large connection lengths in the toroidal section represents an effective transport barrier.

Another feature of the non-uniform escape patterns is their dependence on the safety factor at plasma radius, q_a . To investigate this dependence we calculated for a large number of initial conditions at the tokamak wall uniformly poloidally distributed the connection length of each line (i.e. the number of toroidal turns for the line to return to the tokamak wall). The intervals of points with same connection lengths (expressed in a color scale) are depicted in Figs. 9(a) and 9(b) as a function of q_a for the mode numbers (8, 2) and (10, 2), respectively, with magnifications shown in Figs. 9(c) and 9(d), respectively. We have varied q_a so as not to change the limiter current I_h , hence we have instead to vary the plasma current I_p ; from $I_h/I_p = 0.024$ for $q_a = 3.0$, to $I_h/I_p = 0.040$ for $q_a = 5.0$ for mode number (8, 2) and from $I_h/I_p = 0.010$ for $q_a = 3.0$, to $I_h/I_p = 0.017$ for $q_a = 5.0$ for mode number (10, 2).

We can identify in Figs. 9(a) to 9(d) boomerang-shaped regions for several connection lengths interval, similar to the measurements performed in the tokamak TEXTOR [31]. The sequence of boomerangs are associated to the line stickiness and the escape channels to the wall. The former depends on the last remnant island chain, while the latter is determined by the remnant external island chain around the last remnant island chain on the plasma edge [31,32]. As discussed in Ref. [31,32], the structures (wave-like disturbances) in Figs. 8 and 9 are caused by the heteroclinic tangles associated to the hyperbolic points of the dominant islands.

An empirical observation related to the distribution of magnetic field lines incident on the tokamak wall is the so-called magnetic footprint. In our procedure this is determined by the deposition pattern of the field lines from the chaotic region on the wall. A poloidal distribution of the magnetic footprints shown in Figs. 10(a) and 10(b). The histograms in these figures are obtained by multiplying the number of the lost field lines by their connection lengths for perturbation currents of $I_h/I_p = 0.040$ for a mode number (8, 2), and $I_h/I_p = 0.017$ for a mode number (10, 2). The comparison of Figs. 10(a) and 10(b) indicate that (10, 2) chaotic limiter induces a spread distribution of field lines on the wall. Thus, the arrangement (10, 2) is more adequate for the chaotic limiter since it avoids a high concentration of the field lines with high connection lengths which could carry high energetic particles from the plasma bulk to the wall.

4. Conclusions

In this work we applied the Lagrangian chaos theory, considering typical parameters of fusion plasmas confined in tokamaks. We discussed two effects observed at the plasma edge, namely, the chaotic anomalous particle transport from the $\mathbf{E} \times \mathbf{B}$ drift motion, as well as the distribution of chaotic magnetic field lines at the wall.

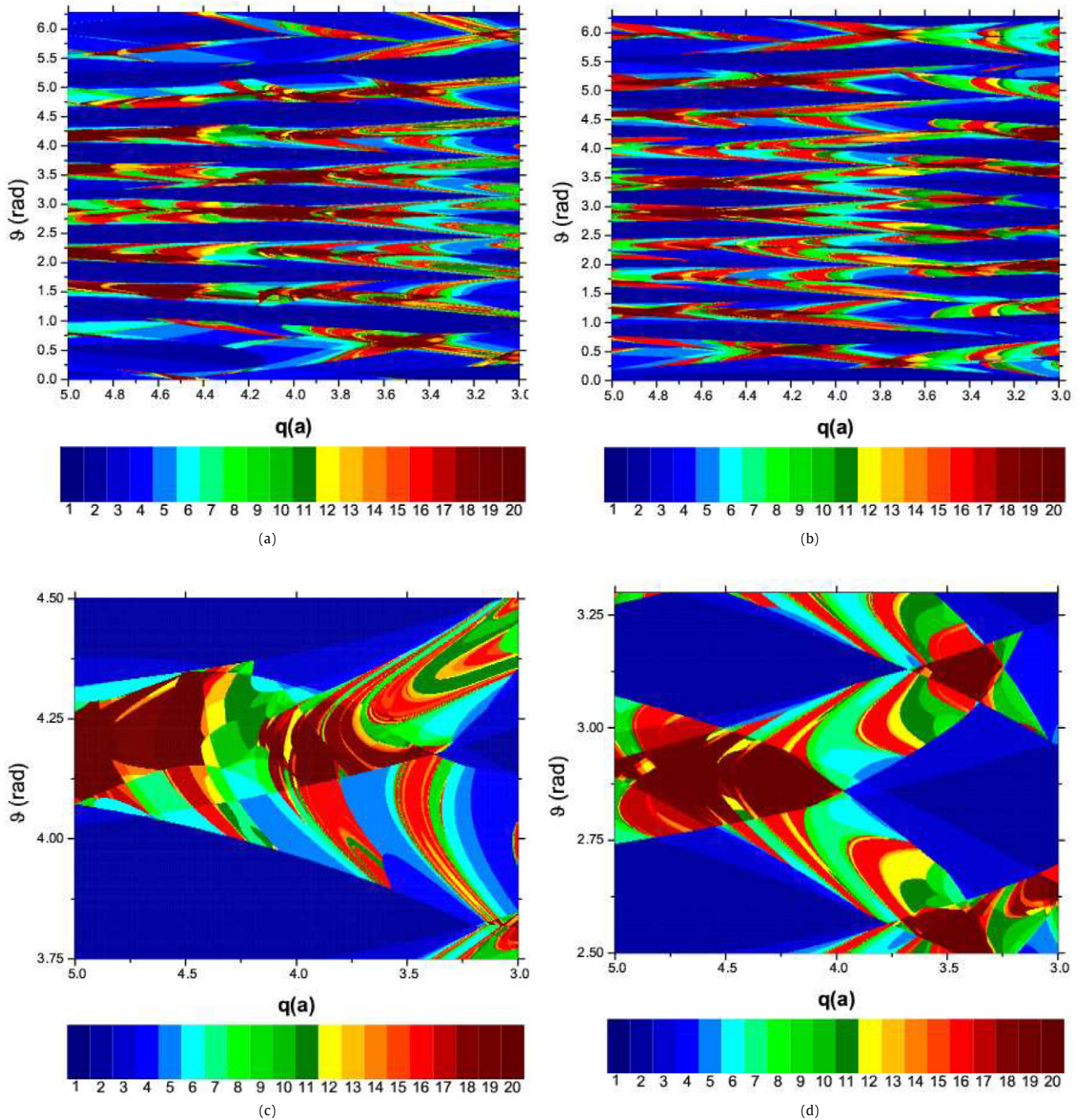


Fig. 9. Intervals of same connection lengths computed at the tokamak wall, as a function of the edge safety factor, corresponding to the Poincaré section shown in Figs. 7(a) and 7(b). (c) and (d) are magnifications of a selected region in (a) and (b), respectively.

Initially, we explored a dynamical mechanism by which the particle transport is achieved and showed how alterations on the electric field radial profile at the plasma edge can modify this transport within this region. Thus, the phase space can be strongly ergodized by this process within the region where the trapping parameter vanishes. On the other hand, by increasing the trapping parameter a particle transport barrier can appear at this region.

Finally, we analyzed the escape of chaotic magnetic field lines due to resonant perturbations created at the plasma edge by an ergodic limiter. For the numerical analysis we considered pertur-

bations with different mode numbers. The field line mappings indicate that limiters with high m are more adequate to reduce the plasma wall interaction. For example, limiters with (8, 2) and (10, 2) mode numbers create more escape channels than those limiters with (4, 1) and (5, 1). Moreover, we showed that the (10, 2) configuration is more appropriate than (8, 2) configuration once the former presents a more scattered escape pattern convenient to reduce the plasma wall interaction. We showed that the number and the distribution of the escape channels are determined by the mean width of the chaotic region and the resonance from which it starts.

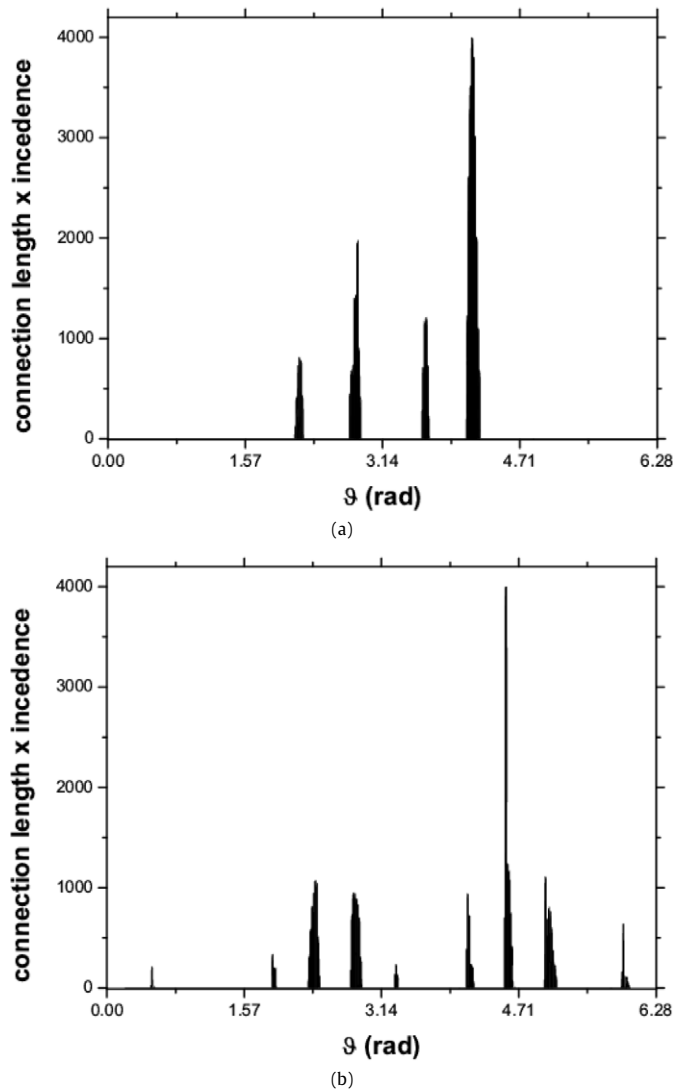


Fig. 10. Histograms for the number of escaping field lines times their connection lengths, corresponding to the Poincaré sections shown in Figs. 7(a) and 7(b).

Acknowledgements

This work was made possible with partial financial support of the following agencies: CNPq, CAPES, FAPESP, and Fundação Araucária.

References

- [1] R.D. Hazeltine, J.D. Meiss, Plasma Confinement, Addison-Wesley, Reading, MA, 1992.
- [2] A.H. Boozer, Rev. Mod. Phys. 76 (2005) 1071.
- [3] M.W. Jakubowski, O. Schmitz, S.S. Abdullaev, S. Brezinsek, K.H. Finken, A. Krämer-Flecken, M. Lehnen, U. Samm, K.H. Spatschek, B. Unterberg, R.C. Wolf, Phys. Rev. Lett. 96 (2006) 0350041.
- [4] T.E. Evans, R.A. Moyer, J.G. Watkins, P.R. Thomasd, T.H. Osbornea, J.A. Boedob, M.E. Fenstermachere, K.H. Finken, R.J. Groebnera, M. Grothe, J. Harrisg, G.L. Jacksona, R.J. La Hayea, C.J. Lasniere, M.J. Schaffera, G. Wangh, L. Zengh, J. Nucl. Mat. 337–339 (2005) 691.
- [5] S.C. Mccool, A.J. Wootton, A.Y. Aydemir, R.D. Bengtson, J.A. Boedo, R.V. Bravenec, D.L. Brower, J.S. Degrassie, T.E. Evans, S.P. Fan, J.C. Forster, M.S. Foster, K.W. Gentle, Y.X. He, R.L. Hickock R, G.L. Jackson, S.K. Kim, M. Kotschenreuther, N.C. Luhmann, W.H. Miner, N. Ohyabu, D.M. Patterson, W.A. Peebles, P.E. Phillips, T.L. Rhodes, B. Richards, C.P. Ritz, D.W. Ross, W.L. Rowan, P.M. Schoch, B.A. Smith, J.C. Wiley, X.H. Yu, S.B. Zheng, Nucl. Fusion 29 (1989) 547.
- [6] D.E. Post, R. Behrisch, Physics of Plasma-Wall Interactions in Controlled Fusion, Plenum Press, New York, 1986.
- [7] R. Parker, G. Janeschitz, H.D. Pacher, D.E. Post, S. Chiochio, G. Federici, P. Ladd, J. Nucl. Mat. 241–243 (1997) 1.
- [8] P.C. Stangeby, The Plasma Boundary of Magnetic Fusion Devices, IOP Publishing, Bristol, 2000.
- [9] W. Horton, Rev. Mod. Phys. 71 (1999) 735.
- [10] A.J. Lichtenberg, M.A. Lieberman, Regular and Chaotic Motion, 2nd ed., Springer-Verlag, New York, 1992.
- [11] M.V.A.P. Heller, I.L. Caldas, A.A. Ferreira, E.A.O. Saettone, A. Vannucci, I.C. Nascimento, J.H.F. Severo, Czech. J. Phys. 55 (2005) 265.
- [12] T.E. Evans, M. Goniche, A. Grosman, D. Guilhem, W. Hess, J.-C. Vallet, J. Nucl. Mat. 196–198 (1992) 421.
- [13] M.W. Jakubowski, S.S. Abdullaev, K.H. Finken, the TEXTOR Team, Nuclear Fusion 44 (2004) S1.
- [14] T.E. Evans, R.K.W. Roeder, J.A. Carter, B.I. Rapoport, Contrib. Plas. Phys. 44 (2004) 235.
- [15] H. Kantz, P. Grassberger, Physica D 17 (1985) 75.
- [16] L. Poon, J. Campos, E. Ott, C. Grebogi, Int. J. Bifurcation Chaos Appl. Sci. Eng. 6 (1996) 251.
- [17] W. Horton, Plas. Phys. Contr. Fus. 27 (1985) 937.
- [18] I. Osipenkov, P.J. Morrison, Diffusion in chaotic systems, Tech. Rep. IFSR 885, Univ. Texas Austin, April 2000.
- [19] A.F. Marcus, T. Kroetz, M. Roberto, I.L. Caldas, E.C. da Silva, R.L. Viana, Z.O. Guimarães-Filho, Nucl. Fusion 48 (2008) 024018; See also: A.F. Marcus, I.L. Caldas, Z.O. Guimarães-Filho, P.J. Morrison, W. Horton, I.C. Nascimento, Yu.K. Kuznetsov, Phys. Plasmas 15 (2008) 112304.
- [20] D. del Castillo-Negrete, J.M. Greene, P.J. Morrison, Physica D (Amsterdam) 100 (1997) 311.
- [21] C.P. Ritz, R.V. Bravenec, P.M. Schoch, R.D. Bengtson, J.A. Boedo, J.C. Forster, K.W. Gentle, Y. He, R.L. Hickok, Y.J. Kim, H. Lin, P.E. Phillips, T.L. Rhodes, W.L. Rowan, P.M. Valanju, A.J. Wootton, Phys. Rev. Lett. 62 (1989) 1844.
- [22] P.J. Morrison, Rev. Mod. Phys. 70 (1998) 467.
- [23] F. Karger, K. Lackner, Phys. Letters A 61 (1977) 385.
- [24] Ph. Ghendrih, M. Bécoulet, L. Colas, A. Grosman, R. Guirlet, J. Gunn, T. Loarer, A. Azéroual, V. Basiuk, B. Beaumont, A. Bécoulet, P. Beyer, S. Brémond, J. Bucalossi, H. Capes, Y. Corre, L. Costanzo, C. De Michelis, P. Devynck, S. Féron, C. Friant, X. Garbet, R. Giannella, C. Grisolia, W. Hess, J. Hogan, L. Ladurelle, F. Laugier, G. Martin, M. Mattioli, B. Meslin, P. Monier-Garbet, D. Moulin, F. Nguyen, J.-Y. Pascal, A.-L. Pecquet, B. Pégourié, R. Reichle, F. Saint-Laurent, J.-C. Vallet, M. Zabiégo, Tore Supra Team, Nucl. Fusion 42 (2002) 1221.
- [25] C.J.A. Pires, E.A. O Saettone, M.Y. Kucinski, A. Vannucci, R.L. Viana, Plas. Phys. Contr. Fus. 47 (2005) 1609.
- [26] E.C. da Silva, I.L. Caldas, R.L. Viana, IEEE Trans. Plas. Sci. 29 (2001) 617.
- [27] S.S. Abdullaev, J. Phys. A 32 (1989) 2745; See also S.S. Abdullaev, Construction of Mappings for Hamiltonian Systems and Their Applications, Springer-Verlag, Berlin, 2006.
- [28] P.M. Morse, H. Feshbach, Methods of Theoretical Physics, vol. 2, McGraw-Hill, New York, 1953.
- [29] M.Y. Kucinski, I.L. Caldas, L.H.A. Monteiro, V. Okano, J. Plas. Phys. 44 (1990) 303.
- [30] M.W. Jakubowski, S.S. Abdullaev, K.H. Finken, M. Lehnen, TEXTOR Team, J. Nucl. Mat. 337–339 (2005) 176.
- [31] A. Wingen, K.H. Spatschek, S.S. Abdullaev, Contr. Plas. Phys. 45 (2005) 500.
- [32] T. Kroetz, M. Roberto, E.C. da Silva, I.L. Caldas, R.L. Viana, Phys. Plasmas 15 (2008) 092310.